#703

Coherent Control of Multidimensional Nonlinear Optical Signals with Shaped Laser Pulses

Dmitri V. Voronine[1], Darius Abramavicius[2], and Shaul Mukamel[2]

[1]Fakultät für Physik, Universität Bielefeld, Bielefeld, Germany
E-mail: dmitri.voronine@gmail.com
[2]Department of Chemistry, University of California, Irvine, Irvine, USA

Multidimensional nonlinear optical signals provide snapshots of electronic and vibrational dynamics in a variety of synthetic and biological systems [1, 2]. Spreading the optical signals in several dimensions increases the spectral feature resolution and provides a better understanding of processes involving structural changes on an ultrafast time scale. However, due to residual spectral congestion a combination of expensive modeling and sophisticated experimental techniques are required to obtain insight into ultrafast spatiotemporal dynamics in complex systems [3].

Adaptive laser pulse shaping was shown to enhance weak cross peaks and improve resolution of simulated multidimensional nonlinear optical spectra of excitons in a model porphyrin dimer [4]. Here we simplify the simulations by using the formalism which takes into account the finite pulse shape but does not require performing multiple integrations for the calculation of the nonlinear response [5]. The coherent third-order nonlinear optical experimental scheme is shown in Figure 1a. The system interacts with three temporally separated laser pulses and the signal is emitted in the phase-matching direction k_4 and heterodyned with the fourth laser pulse. We consider the $k_I = -k_1+k_2+k_3$ signal which is described by the Feynman diagrams shown in Figure 1b which may be represented using the simplified sum-over-state expressions Eqs. 1 – 3.

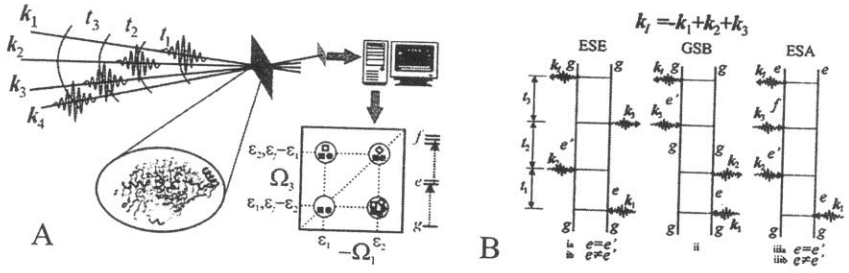

Fig. 1. (A) Coherent third-order nonlinear optical experiment. The four laser pulses are ordered in time; the signal is generated in the phase-matching direction k_4. Data processing of time-domain signals and their parametric dependence on the three delays t_1, t_2, and t_3 generate multidimensional spectrograms [1,2]. (B) Feynman diagrams for the signal generated in the direction $k_I = -k_1+k_2+k_3$; ESE = excited-state emission, ESA = excited-state absorption, and GSB = ground-state bleaching. Population diagrams are labeled ia, ii and iiia, and coherence diagrams are labeled ib and iiib.

$$S_{\mathbf{k}_I,i}(\Omega_3,\Omega_2,\Omega_1) = -\sum_{ee'} \frac{\left(\mu^*_{e'g}\cdot E^*_3(\omega_{e'g}-\omega_3)\right)\left(\mu_{eg}\cdot E_3(\omega_{eg}-\omega_3)\right)\left(\mu_{e'g}\cdot E_2(\omega_{e'g}-\omega_2)\right)\left(\mu^*_{eg}\cdot E^*_1(\omega_{eg}-\omega_1)\right)}{\hbar^3(\Omega_3-\xi_{e'g})(\Omega_2-\xi_{e'e})(\Omega_1-\xi_{ge})}, \quad (1)$$

$$S_{\mathbf{k}_I,ii}(\Omega_3,\Omega_2,\Omega_1) = -\sum_{ee'} \frac{\left(\mu^*_{e'g}\cdot E^*_3(\omega_{e'g}-\omega_3)\right)\left(\mu_{e'g}\cdot E_3(\omega_{e'g}-\omega_3)\right)\left(\mu_{eg}\cdot E_2(\omega_{eg}-\omega_2)\right)\left(\mu^*_{eg}\cdot E^*_1(\omega_{eg}-\omega_1)\right)}{\hbar^3(\Omega_3-\xi_{e'g})(\Omega_2+i\eta)(\Omega_1-\xi_{ge})}, \quad (2)$$

$$S_{\mathbf{k}_I,iii}(\Omega_3,\Omega_2,\Omega_1) = \sum_{fee'} \frac{\left(\mu^*_{fe}\cdot E^*_3(\omega_{ef}-\omega_3)\right)\left(\mu_{fe'}\cdot E_3(\omega_{fe'}-\omega_3)\right)\left(\mu_{e'g}\cdot E_2(\omega_{e'g}-\omega_2)\right)\left(\mu^*_{eg}\cdot E^*_1(\omega_{eg}-\omega_1)\right)}{\hbar^3(\Omega_3-\xi_{fe})(\Omega_2-\xi_{e'e})(\Omega_1-\xi_{ge})}, \quad (3)$$

where $S_{kI}(\Omega_1,\Omega_2,\Omega_3)$ are the contributions of various Feynman diagrams to the third-order heterodyne-detected $\mathbf{k}_I$ signal, μ are transition dipoles, E are complex electric field envelopes with ω_i center frequencies, ω_{eg} are interband frequencies, and $\xi_{ge} = \omega_{ge}$ - i γ_{ge} are complex frequencies with phenomenological dephasing rates γ_{ge} . These expressions allow tuning parameters of the electric fields of the four laser pulses such as their carrier frequencies, phases, bandwidths and envelopes to optimize third-order signals. Such a strategy may be used for designing "smart" pulse sequences more efficiently and understanding the resulting optimal pulse shapes. This is usually difficult in adaptive pulse shaping where optimal pulses are complex.

We performed multiparameter coherent control of simulated 2D $\mathbf{k}_I$ signals of excitons in the photosynthetic Fenna-Matthews-Olson (FMO) complex from green sulfur bacterium *Chlorobium tepidum* at 77 K. The simulation details have been reviewed elsewhere [2]. 2D spectra obtained with all four unshaped transform-limited Gaussian laser pulses consist of 7 overlapping diagonal peaks corresponding to 7 single-exciton eigenstates and a number of weak cross peaks (Figure 2b, top). The diagonal peaks are the dominant spectral features which overlap with cross peaks and further decrease their resolution.

To control 2D spectral features resulting from interference of various Liouville space pathways we varied the linear chirp of the first and third laser pulses. Wigner spectrograms show the unshaped (top), positively (middle) and negatively (bottom) chirped pulses in Figure 2a. By varying the time delays of various frequencies of the first laser pulse which creates the coherence between different excitons we can control the shape of the initial exciton wave packets and their subsequent evolution. The third laser pulse interacts with the system and reverses the coherent dynamics. Therefore, by applying the same amount of positive linear chirp on both the first and the third laser pulses results in a similar 2D spectrum (Figure 2b, bottom) to that of the spectrum with all four unshaped pulses (Figure 2a, top). The spectral patterns are similar but the spectrum with shaped laser pulses reveals stronger cross peaks which are highlighted by stars. However, by applying the opposite chirp to the first and third pulses results in significant differences of the spectra such as switching the signs of the high energy diagonal peaks in the dispersive (left column) and the absorptive (right column) parts of the spectra (shown by arrows in Figure 2b, middle). The cross peaks are also enhanced even more in comparison with the shaped similarly chirped pulses.

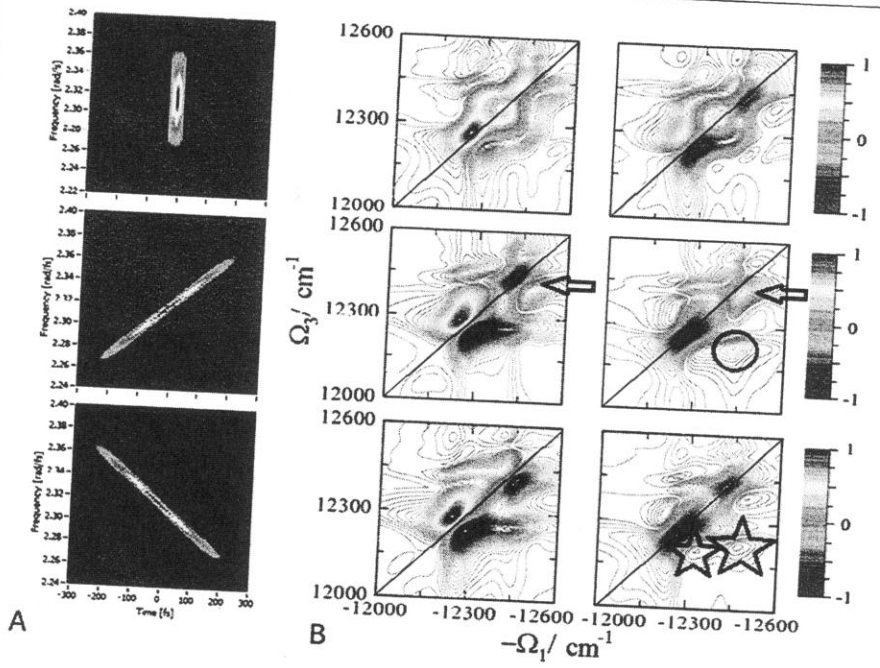

Fig. 2. (A) Wigner spectrog-rams of the unshaped Gaussian (top), and shaped positively (middle) and negatively (bottom) chirped laser pulses. (B) The corresponding real (left column) and imaginary (right column) parts of the simulated normalized k_I 2D spectra of the photosynthetic Fenna-Matthews-Olson complex from the green sulfur bacterium *Chlorobuim tepidum* at 77 K: (top) 2D spectra with all four unshaped Gaussian laser pulses; (middle) with 1st positively chirped, 2nd unshaped Gaussian, 3rd negatively chirped, and 4th unshaped Gaussian pulse; (bottom) with 1st positively chirped, 2nd unshaped Gaussian, 3rd positively chirped, and 4th unshaped Gaussian pulse.

We have demonstrated how simplified calculations of multidimensional nonlinear optical signals of photosynthetic excitons may be used to design novel pulse sequences to optimize spectral features. Applying opposite chirp on the first and third laser pulses allows controlling exciton dynamics revealed by interference of Liouville space pathways and probing hidden features of multidimensional nonlinear response.

1. S. Mukamel, Principles of Nonlinear Optical Spectroscopy; Oxford University Press: New York, 1995.
2. D. Abramavicius, B Palmieri, D. V. Voronine, F. Sanda, and S. Mukamel, Chem. Rev. **109**, 2350, 2009.
3. T. Brixner, J. Stenger, H. M. Vaswani, M. Cho, R. E. Blankenship, and G. R. Fleming, Nature **434**, 625, 2005.
4. D. V. Voronine, D. Abramavicius, and S. Mukamel, J. Chem. Phys. **126**, 044508, 2007.
5. I. V. Schweigert, and S. Mukamel, Phys. Rev. A **77**, 033802, 2008.